Ordered Carbides

DOI: 10.1002/anie.201206183

Access to Ordered Porous Molybdenum Oxycarbide/Carbon Nanocomposites**

*Thomas Lunkenbein, Dirk Rosenthal, Torsten Otremba, Frank Girgsdies, Zihui Li, Hiroaki Sai, Carina Bojer, Gudrun Auffermann, Ulrich Wiesner, and Josef Breu**

Heterogeneous catalysis is still dominated by metals, metal oxides, and metal sulfides.[1] However, additional demands for more sophisticated, efficient, and economical processes require alternative catalytic materials. For instance, in industrial catalytic processes there is a growing interest in substituting rare and expensive noble metal catalysts by cheap and abundant transition-metal carbide (TC) materials. For this reason, TCs have attracted considerable interest in current academic catalysis research. It has for example, been demonstrated by Levy and Boudart that the combination of Group 6 transition metals and carbon can result in Pt-like properties with respect to activity, selectivity, and resistance against poisoning.[1,2] In particular, in catalytic reactions involving the transformation of C–H bonds of hydrocarbons, that is, dehydrogenation, hydrogenation, and hydrogenolysis, TCs received a great deal of attention.[3]

Applying conventional carburization methods, porous TCs with high specific surface areas are difficult to obtain. Standard metallurgy approaches involve reaction of the metals with carbon at temperatures above 1200 °C.[4] This inevitably yields bulk TCs with low surface area and mediocre catalytic activity. Exploration of the true potential of TCs requires the development of appropriate synthesis techniques leading to TCs with nanoscale particle size, high surface area, and large pore volumes.[5] For instance, studies on the accessibility of the active sites by CO chemisorption experiments reveal an CO uptake between 178 and 950 $\mu mol\,g^{-1}$.[6] High-surface-area TCs have been reported using a temperature programmed reduction,[6] high-temperature decomposition,[7] or carbothermal reduction.[8] Although these preparation methods deliver high surface area and catalytically active TCs,[9] the resulting carbides do not feature ordered and uniform pores that might optimize mass transport.[10]

Techniques for organizing TCs on the mesoscale using inorganic or organic matrices are scarce. Ordered mesoporous TCs have been reported by exotemplating of polyoxometalates into mesoporous silica followed by carburization using an additional carbon source, such as CO or CH_4.[11] Ordered micro-/mesoporous TC/carbon (TC/C) nanocomposites with total pore volumes of 0.43–0.49 $cm^3\,g^{-1}$ were synthesized by endotemplating of pre-synthesized, stabilized TO_x nanoparticle suspensions into a pluronics template followed by carbothermal reduction.[12] For successful carburization additional carbon sources and/or curing steps were required, rendering the process rather complex.

Aside from catalysis, such hierarchical porous TC/C nanocomposites (micropores in the wall of mesopores) have been shown to be excellent precursors for super capacitors.[12d] In brief, ordered mesoporous channels support penetration and transport of the electrolyte. The open space is an essential feature for highly efficient capacitors. Simultaneously, micropores embedded in the walls of mesopores provide additional space for charge storage.[13]

TC/C nanocomposites are, however, not only superior to pure TCs in super capacitor applications, their catalytic activity and stability is also advanced.[14] The development of

[*] T. Lunkenbein, C. Bojer, Prof. Dr. J. Breu
Anorganische Chemie I
Universität Bayreuth
Universitätsstrasse 30, 95440 Bayreuth (Germany)
E-mail: josef.breu@uni-bayreuth.de
Homepage: http://www.ac1.uni-bayreuth.de
Dr. D. Rosenthal, Dr. F. Girgsdies
Fritz-Haber-Institut der Max-Planck-Gesellschaft
Farradayweg 4–6, 14195 Berlin (Germany)
Z. Li, H. Sai, Prof. Dr. U. Wiesner
Materials Science & Engineering
Cornell University
Ithaca, NY 14853 (USA)
T. Otremba
Institut für Chemie
Technische Universität Berlin
Strasse des 17. Juni 124
10623 Berlin (Germany)
Dr. G. Auffermann
Max-Planck Institut für Chemische Physik fester Stoffe
Nöthnitzer Strasse 40
01187 Dresden (Germany)

[**] This work was supported by the Deutsche Forschungsgemeinschaft (DFG) within the Collaborative Research Center (SFB) 840 (Project A7). T.L. acknowledges the international graduate school of the ENB "Structures, Reactivity and Properties of Metal Oxides" for a fellowship. Z.L. was supported by the U.S. Department of Homeland Security under Cooperative Agreement Number 2009-ST-108-LR0004. H.S. was supported through the National Science Foundation (NSF) grant DMR-1120296. The X-ray equipment was supported by Department of Energy grant DEFG-02-97ER62443. CHESS was supported by the NSF and NIH-NIGMS via DMR-0225180. We thank Prof. Sol Gruner (Department of Physics, Cornell University) for letting us acquire some of the SAXS patterns in his lab. Prof. Dr. Rüdiger Kniep is gratefully acknowledged for the support with elemental analysis. We also thank Prof. Dr. Axel H. E. Müller for ensuring easy access to its anionic polymerization reactors. Dr. Andrey Tarasov is acknowledged for thermogravimetric measurements. Klaus Friedel-Ortega, Dr. Annette Trunschke, and Prof. Dr. Robert Schlögl are acknowledged for fruitful discussions and support with heat treatment and TEM equipment.

Supporting information for this article is available on the WWW under http://dx.doi.org/10.1002/anie.201206183.

a general method for direct access to ordered mesoporous TC/C nanocomposites with TC walls, uniform and accessible pores, and high porosity is consequently highly desirable.

Herein we describe a direct route towards hexagonally ordered mesoporous molybdenum carbide/carbon (MoC/C) nanocomposites by endotemplating followed by subsequent carbothermal reduction in an inert atmosphere. Molybdophosphoric acid ($H_3PMo_{12}O_{40}$; H_3PMo) was adopted as molybdenum precursor. A structure-directing agent (SDA) that is particularly rich in sp^2 carbon was applied, namely poly(butadiene-*block*-2-vinylpyridine) (PB-b-P2VP), which at the same time served as carbon source in the carburization reaction. As we will show, key to successful generation of mesoporous materials without loss of the block copolymer directed mesostructure was heat treatment of the as-made composites to temperatures above 700 °C.

Scheme 1 summarizes our approach. After synthesis of the block copolymer PB-b-P2VP (30 kg mol^{-1}, 26 wt % P2VP, PDI 1.02) and composites (see the Supporting Information for details), structural assignment of the resulting mesostructured PB-b-P2VP/H_3PMo nanocomposites was accomplished

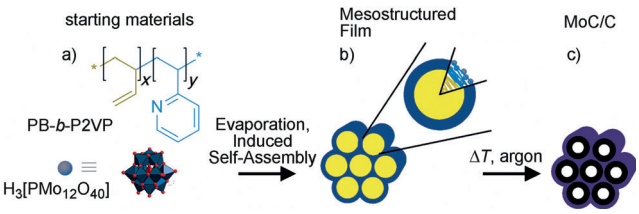

Scheme 1. Illustration of the synthesis of MoC/C: a) Chemical structure of PB-b-P2VP (top) and H_3PMo (bottom). The indices *x* and *y* denote the degrees of polymerization (DP) of the PB ($x = 411$) and P2VP units ($y = 75$). b) Inverse hexagonal mesophase obtained after solvent evaporation. c) MoC/C with retained mesostructure after heat treatment (740 °C) in an argon atmosphere.

by small-angle X-ray scattering (SAXS) measurements (Figure 1). In Figure 1a, the expected peak positions for higher order Bragg reflections of a hexagonal lattice centered around the first-order maximum at angular positions equal to the ratio of $1:\sqrt{3}:2:\sqrt{7}:3:\sqrt{12}:\sqrt{13}$ are indicated by vertical ticks, and suggest a morphology of hexagonally ordered

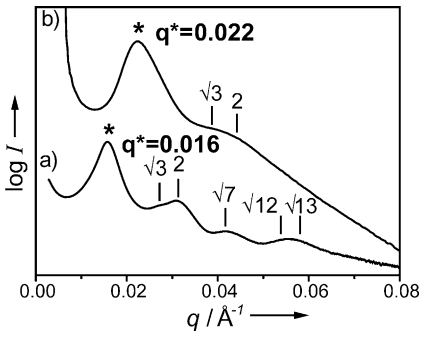

Figure 1. SAXS patterns of a) as-synthesized PB-b-P2VP/H3PMo nanocomposite and b) MoC/C. Expected peak positions for hexagonal lattices are indicated by vertical lines.

cylinders. The corresponding spacing (d-spacing) is 39 nm. A hexagonal mesostructure was further corroborated by bright-field TEM measurements (Figure 2a,b). The TEM images show the inverse hexagonal mesostructure of the PB-b-P2VP/H_3PMo nanocomposite with a PB pore diameter of (27.0 ± 1.6) nm and a wall thickness of (9.0 ± 1.1) nm. The high-resolution (HR) TEM image in Figure 2b shows the good

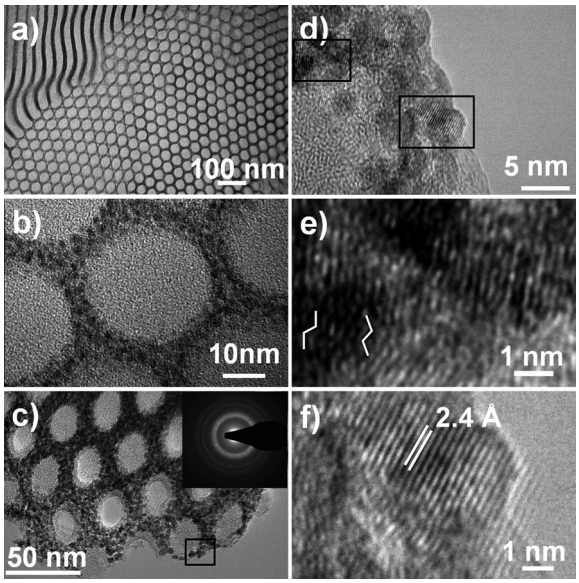

Figure 2. Representative bright-field TEM images of PB-b-P2VP/H_3PMo nanocomposite (a and b) and of MoC/C at different magnifications (c–f). The inset in (c) represents a SAED pattern indicative for nanocrystalline MoO_xC_y. d) Close-up of the area in the black box in (c). The black boxes in (d) denote selected areas of which HR-TEM images (e, top, and f, bottom) were taken. e) displays the chevron-like structure of the vacancies of MoO_xC_y along the [010] zone axis. f) shows a HR-TEM image of a single nanocrystal. The spacing of 2.4 Å is consistent with the (111) plane of MoO_xC_y.

dispersion of discrete H_3PMo units selectively incorporated into the P2VP walls. The diameter of the monodisperse dark dots was estimated to be 1.2 nm, which is consistent with the reported diameter of H_3PMo clusters (1.1 nm).[15] The good dispersion of the H_3PMo units within the polymeric matrix was further corroborated by the amorphous nature of the powder patterns of as-synthesized PB-b-P2VP/H_3PMo nanocomposites (Supporting Information, Figure S3b).

The catalytic functionality of such hexagonal ordered PB-b-P2VP/H_3PMo nanocomposites can only be achieved if the material can be rendered into mesoporous POM while retaining the mesostructure. However, complete removal of the polymeric matrix resulting in pure mesoporous Keggin-Type polyoxometalates (Keggin POMs) unfortunately is not straightforward for the following reasons: It is well established that unlike rutile nanocrystals, Keggin POMs show almost no tendency to connect covalently to neighboring units by condensation of two hydroxy groups, as the most basic oxygen atoms are the bridging atoms, which are remote from the surface of the cluster. Thus a rigid inorganic framework that prevents the mesostructure to collapse cannot be constructed during pyrolysis of the composite films. Applying

isopoly acids of molybdenum does not solve the problem either: Vapor-phase sintering readily leads to micrometer-sized MoO_3 crystals even at relative moderate temperatures, and the mesostructure is lost. In any case, the preparation of ordered and mesoporous molybdenum compounds is not trivial.

In line with these considerations, original efforts to generate mesoporous materials by heating below 700 °C failed. Below this temperature, the rigid carbon formed in situ hampers access to mesopores. It was only at higher temperatures that as-made composites could be converted to mesoporous materials without loss of the mesostructure. To understand and explain the chemical reactions involved upon heat treatment and to verify a mesoporous material we examined the mesostructured PB-b-P2VP/H_3PMo nanocomposites in more detail, conducting thermogravimetric analysis coupled with mass spectrometry (TGA-MS) in a He atmosphere (Supporting Information, Figure S4). TG measurements showed an almost continuous mass loss below 700 °C, whereas above 700 °C a steep decay in the TG signal of 17 wt % was observed. The mass loss below 700 °C could be attributed to the pyrolysis of the diblock copolymer and the formation of the rigid carbon scaffold.[16] Above 700 °C the MS analysis showed the release of CO_2 and CO, indicating the reduction of the molybdenum oxide species by parts of the carbonaceous material.[4]

During this heat treatment, several processes occur: The sp^2-hybridized carbon is converted into a rigid carbonaceous scaffold; the H_3PMo clusters decompose and parts of the carbonaceous material react with the molybdenum centers to form molybdenum carbides, while elemental analysis (EA) revealed that the phosphorous remains in the resulting MoC/C nanocomposite (Supporting Information, Table S1). This was confirmed by amounts of Mo_3P detectable by PXRD in material being annealed at 800 °C for 100 min.

To generate mesoporous materials, the as-synthesized inverse hexagonal PB-b-P2VP/H_3PMo nanocomposites were heat-treated under argon atmosphere in a tube furnace. Composites were heated to 740 °C; at this temperature, the carbide nanocrystals formed in situ arrange into a woven microstructure that, together with the remaining rigid carbon scaffold, assures the retention of the hexagonal mesostructure.

Structural characterization of the resulting MoC/C nanocomposites revealed preservation of the ordered mesostructure. SAXS patterns (Figure 1 b) of heat-treated composites show a first-order maximum with corresponding d-spacing of 28.6 nm and a broader higher order reflex indicating some degree of long-range order. Expected higher-order reflections for a hexagonal lattice at angular position of $\sqrt{3}$ and 2 of the first-order maximum are indicated by ticks above the broad scattering feature in Figure 1 b. Assuming a hexagonal lattice the shift of the primary *10* reflection to higher values of the scattering vector q implies a decrease of the cell dimension by 28 %. The structural assignment to a hexagonal lattice was corroborated by TEM studies (Figure 2 c–f).

TEM micrographs of MoC/C exhibit a well-defined 2D hexagonal mesostructure (Figure 2 c) with pore diameters of (19.3 ± 4.0) nm and wall thicknesses of (13.1 ± 1.6) nm consistent with the observed d-spacing of the SAXS patterns (28.6 nm). TEM images also revealed the presence of narrowly size-distributed carbide nanoparticles well-dispersed in the carbon matrix and exhibiting an average diameter of roughly 4 nm. During heat treatment, the randomly distributed H_3PMo units within the P2VP matrix produced a large number of carbide nuclei leading to a rather small particle size. The rigid carbon scaffold formed in situ is capable of preventing collapse of the mesostructures upon heat treatment, and carbide formation can clearly be identified around the pores in TEM (Supporting Information, Figure S5).

Powder X-ray diffraction (PXRD) patterns of the heat-treated nanocomposites showed two broad reflections at angular positions of 37° and 43° (Supporting Information, Figure S3c, S6aA) attributed to the (111) and (200) planes of a face-centered cubic (fcc) arrangement of MoC_{1-x} or molybdenum oxycarbide (MoO_xC_y). The diffusive selected-area electron diffraction pattern (SAED, inset in Figure 2 cxfigr2 >) further corroborated the formation of fcc-type carbide species. It has recently been highlighted that oxycarbides and fcc-MoC_{1-x} possess similar PXRD patterns.[17] Figure 2 f shows a HR-TEM image of a single nanocrystal. The spacing of 2.4 Å corresponds well with the (111) plane of MoC_{1-x} or MoO_xC_y. To clarify the nature of the carbide phase, a combined analytical sequence of EA, TGA-MS in a hydrogen–argon mixture (95:5 v/v), and HR-TEM measurements of MoC/C were conducted. The presence of considerable amounts of oxygen (EA; Supporting Information, Table S1) and the concomitant release of CO and CH_4 in the TGA (additional weight loss of 6 wt %) as detected by MS profiles (Supporting Information, Figure S7) were more in line with an oxycarbide species. Furthermore, HR-TEM images showed a chevron-like structure (Figure 2 e). This structure is well-known to result from atom vacancies in the [010] zone axis of crystalline MoO_xC_y.[18]

Nitrogen physisorption measurements (Figure 3 a) of porous MoC/C exhibited a type I isotherm with a type H4 hysteresis. The specific surface area of $133\ m^2 g^{-1}$ was determined by applying the BET equation. As micropores were detected, the recommendations of Rouquerol et al. were followed for calculating the BET surface area.[19] Nonlocal density functional theory (NLDFT, slit/cylindrical pore kernel) was adopted to determine the pore size distribution and pore volumes. NLDFT analysis of nitrogen physisorption isotherms showed the presence of both micro- and mesopores in MoC/C (Figure 3 b). The estimated cumulative pore volume was $0.085\ cm^3 g^{-1}$. Approximately half of the total volume, $0.043\ cm^3 g^{-1}$, could be attributed to micropores (Supporting Information, Figure S8). Four peaks at diameters of 0.68 nm, 1.27 nm, 3.79 nm, and 5.30 nm were observed. Most likely, the micropore peaks are related to holes in the carbon scaffold. At first sight, the TEM images might suggest a rather uniform pore size of mesopores in the range of 19.3 nm. The pore size distribution, however, rapidly decayed after 5.3 nm. Only very little pore volume stretches the range up to a maximum of 17.5 nm. As also seen in TEM micrographs (Figure 2 c and Supporting Information, Figure S5), a rigid amorphous carbon scaffold lines the walls, resulting in

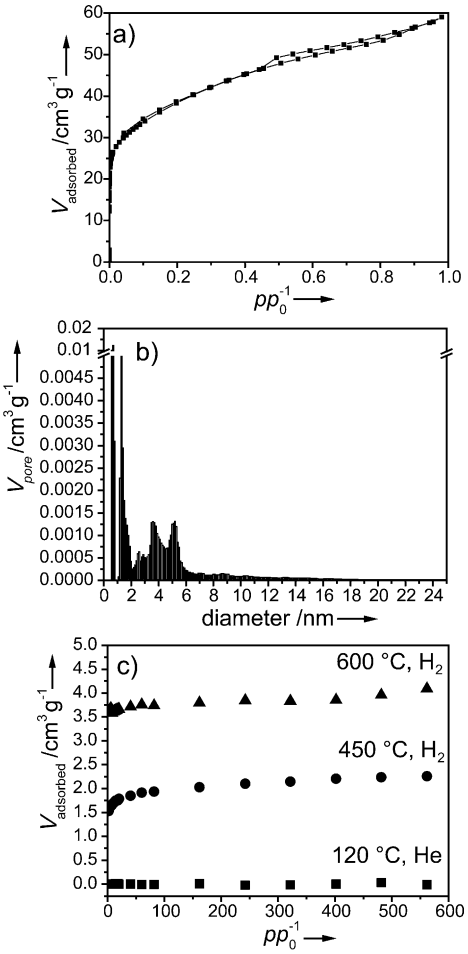

Figure 3. a) Nitrogen physisorption isotherm of MoC/C. b) NLDFT analysis of nitrogen adsorption isotherms of the micropore and mesopore distribution of MoC/C. c) Chemisorption curves for the irreversible CO uptake of MoC/C after different pretreatments: in He atmosphere at 120 °C (squares), in pure H_2 atmosphere at 450 °C (circles) and in pure H_2 atmosphere at 600 °C (triangles). In all cases, holding times were 2 h.

the size limitation and partial blocking of the voids. The hierarchical pore structure in which micropores are incorporated into the walls of ordered mesopores provided the high specific surface area.

To further test the concept of rigid carbon lining the walls, Raman spectroscopy was performed (Supporting Information, Figure S9). The rigid carbon scaffold not only embedded the large number of MoO_xC_y nanocrystals, but also retained the hexagonal order of the mesopores. However, it also passivated the molybdenum oxycarbide centers by acting as a barrier to accessing reactive sites as shown by chemisorption experiments (Figure 3c). When MoC/C was pretreated in a He atmosphere, no CO uptake was detectable (Figure 3c, squares). However, prior exposure of the composite to pure hydrogen atmosphere at 450 °C (Figure 3d, circles) and 600 °C (Figure 3c, triangles) led to an irreversible CO uptake of 84 μmol g^{-1} and 165 μmol g^{-1}, respectively. Hydrogenation and removal of carbon that covered the surface may facilitate diffusion of CO molecules and allow adsorption. Thus, H_2 pretreatment resulted in the modification of the chemisorption properties of the material that may be caused by partial reduction of the oxycarbide surface under formation of Mo_2C (Supporting Information, Figure S6aB) and minor changes in the pore geometry (Supporting Information, Figure S10).

The hexagonal mesostructure was maintained as evidenced by TEM investigations (Supporting Information, Figure S6b). Thus, appropriate pretreatment in a reductive atmosphere could enable a way to uncover carbide centers activating the material for catalysis. To check this hypothesis, activated MoC/C was tested as potential catalyst in the decomposition of NH_3. Preliminary investigations revealed activity of MoC/C in the decomposition reaction of NH_3 (Supporting Information, Figure S11). The activation energy was estimated to be 156 kJ mol^{-1} (Supporting Information, Figure S11b), which is in close agreement with results reported earlier for other molybdenum carbides (151 kJ mol^{-1}).[20]

In summary, we have established a direct path to mesoporous MoC/C nanocomposites by simple high-temperature (> 700 °C) heat treatment of a hexagonally ordered diblock copolymer/heteropoly acid nanocomposite in an argon atmosphere. The diblock copolymer served multiple tasks, that is, as SDA and as carbon source. The H_3PMo units could easily be converted into MoO_xC_y nanoparticles, which were embedded in a porous carbon matrix. The resulting MoC/C nanocomposites exhibited inverse hexagonal order, hierarchical pore structure, and high surface area. These MoO_xC_y nanoparticles could be activated by uncovering them by pretreatment in H_2. MoC/C nanocomposites showed not only activity in catalysis, such as NH_3 decomposition, but the hierachical pore strucure may also render them interesting for super capacitor applications.

Received: August 1, 2012
Published online: November 9, 2012

Keywords: carbides · heterogeneous catalysis · physisorption · polyoxometalates · self-assembly

[1] A. M. Alexander, J. S. J. Hargreaves, *Chem. Soc. Rev.* **2010**, *39*, 4388 – 4401.
[2] R. B. Levy, M. Boudart, *Science* **1973**, *181*, 547 – 549.
[3] a) H. H. Hwu, J. G. Chen, *Chem. Rev.* **2005**, *105*, 185 – 212; b) J. G. Chen, *Chem. Rev.* **1996**, *96*, 1477 – 1498.
[4] A. Hanif, T. Xiao, A. P. E. York, J. Sloan, M. L. H. Green, *Chem. Mater.* **2002**, *14*, 1009 – 1015.
[5] C. Giordano, C. Erpen, W. Yao, M. Antonietti, *Nano Lett.* **2008**, *8*, 4659 – 4663.
[6] a) J. S. Lee, S. T. Oyama, M. Boudart, *J. Catal.* **1987**, *106*, 125 – 133; b) J. S. Lee, L. Volpe, F. H. Riberio, M. Boudart, *J. Catal.* **1988**, *112*, 44 – 53.
[7] H. Preiss, B. Meyer, C. Olschewski, *J. Mater. Sci.* **1998**, *33*, 713 – 722.
[8] M. J. Ledoux, S. Hantzer, C. P. Huu, J. Guille, M. P. Desaneaux, *J. Catal.* **1988**, *114*, 176 – 185.
[9] a) T. Xiao, H. Wang, J. Da, K. S. Coleman, M. L. H. Green, *J. Catal.* **2002**, *211*, 183 – 191; b) M. A. Ecormier, K. Wilson, A. F. Lee, *J. Catal.* **2003**, *215*, 57 – 65.
[10] a) D. L. Li, H. S. Zhou, I. Honma, *Nat. Mater.* **2004**, *3*, 65 – 72; b) F. Hoffmann, M. Cornelius, J. Morell, M. Fröba, *Angew. Chem.* **2006**, *118*, 3290 – 3328; *Angew. Chem. Int. Ed.* **2006**, *45*,

3216 – 3251; c) M. C. Orilall, U. Wiesner, *Chem. Soc. Rev.* **2011**, *40*, 520 – 535; d) F. Schüth, *Angew. Chem.* **2003**, *115*, 3730 – 3750; *Angew. Chem. Int. Ed.* **2003**, *42*, 3604 – 3622; e) M. Hartmann, *Angew. Chem.* **2004**, *116*, 6004 – 6006; *Angew. Chem. Int. Ed.* **2004**, *43*, 5880 – 5882.

[11] a) X. Cui, H. Li, L. Guo, D. He, H. Chen, J. Shi, *Dalton Trans.* **2008**, 6435 – 6440; b) Z. Wu, Y. Yang, D. Gu, Q. Li, D. Feng, Z. Chen, B. Tu, P. A. Webley, D. Zhao, *Small* **2009**, *5*, 2738 – 2749.

[12] a) J. Han, J. Duan, P. Chen, H. Lou, X. Zheng, H. Hong, *ChemSusChem* **2012**, *5*, 727 – 733; b) C. H. Huang, D. Gu, D. Zhao, R. A. Doong, *Chem. Mater.* **2010**, *22*, 1760 – 1767; c) T. Yu, Y. Deng, L. Wang, R. Liu, L. Zhang, B. Tu, D. Zhao, *Adv. Mater.* **2007**, *19*, 2301 – 2306; d) H. J. Liu, J. Wang, C. X. Wang, Y. Y. Xia, *Adv. Energy Mater.* **2011**, *1*, 1101 – 1108.

[13] J. Chmiola, G. Yushin, Y. Gogotsi, C. Portet, P. Simon, P. L. Taberna, *Science* **2006**, *313*, 1760 – 1763.

[14] J. Sun, M. Zheng, X. Wang, A. Wang, R. Cheng, T. Li, T. Zhang, *Catal. Lett.* **2008**, *123*, 150 – 155.

[15] A. Stein, M. Fendorf, T. P. Jarvie, K. T. Müller, A. J. Benesi, T. E. Mallouk, *Chem. Mater.* **1995**, *7*, 304 – 313.

[16] J. Lee, M. C. Orilall, S. C. Warren, M. Kamperman, F. J. Disalvo, U. Wiesner, *Nat. Mater.* **2008**, *7*, 222 – 228.

[17] T. C. Xiao, A. P. E. York, V. C. Williams, H. Al Megren, A. Hanif, X. y. Zhou, M. L. H. Green, *Chem. Mater.* **2000**, *12*, 3896 – 3905.

[18] S. T. Oyama, C. Delporte, C. Pham-Huu, M. J. Ledoux, *Chem. Lett.* **1997**, *9*, 949 – 950.

[19] J. Rouquerol, P. Llewellyn, F. Rouquerol in *Studies in Surface Science and Catalysis Characterization of Porous Solids VII Proceedings of the 7th International Symposium on the Characterization of Porous Solids (COPS-VII), Aix-en-Provence, France, 26 – 28 May 2005* (Ed.: P. L. Llewellyn), Elsevier, Amsterdam, **2007**, pp. 49 – 56.

[20] C. Jeong-Gil, *J. Catal.* **1999**, *182*, 104 – 116.

